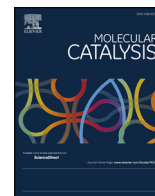




Contents lists available at ScienceDirect

## Molecular Catalysis

journal homepage: [www.elsevier.com/locate/mcat](http://www.elsevier.com/locate/mcat)

# Synthesis and characterization of nanoparticulate silica with organized multimodal porous structure impregnated with 12-phosphotungstic acid for its use in heterogeneous catalysis

Dolores M. Morales, Romina A. Frenzel, Gustavo P. Romanelli, Luis R. Pizzio\*

*Centro de Investigación y Desarrollo en Ciencias Aplicadas "Dr. Jorge J. Ronco" (CINDECA), CCT-La Plata-CONICET, Departamento de Química, Facultad de Ciencias Exactas, Universidad Nacional de La Plata, 47 N° 257 (B1900AJK), La Plata, Argentina*

## ARTICLE INFO

**Keywords:**  
Nanoparticles  
Mesoporous silica  
Phosphotungstic acid  
Benzodiazepines

## ABSTRACT

Mesoporous silica (MESSI) nanoparticles with ordered mesoporous frameworks were successfully obtained using the triblock copolymer P123 as the mesoporous template and agar as micropore former. The agar/TEOS ratio influences the specific surface area ( $S_{\text{BET}}$ ) and the micropore area ( $S_{\text{MIC}}$ ). The  $S_{\text{BET}}$  values increase with the increment of the agar/TEOS ratio used in the synthesis. SAXS (small angle X-ray scattering) patterns and TEM (transmission electron microscopy) images of MESSI samples reveal the presence of a 2D hexagonal mesopore array. The study of all the materials impregnated with PTA by  $^{31}\text{P}$  NMR and FT-IR confirmed the existence of undegraded  $[\text{H}_{3-x}\text{PW}_{12}\text{O}_{40}]^{(3-x)-}$  and  $[\text{PW}_{12}\text{O}_{40}]^{3-}$  anions interacting with the  $=\text{Si}-\text{OH}_2^+$  groups. The potentiometric titration results show that the MESSI-2PTA solids present very strong acid sites and that both the acid strength and the number of sites increase with the increment of the PTA amount in the samples.

The performance of MESSI-2PTA materials as catalysts in the solvent-free synthesis of a series of substituted 3H-1,5-benzodiazepines was evaluated. The yields achieved were high, without formation of by-products resulting from competitive reactions or decomposition products, so the prepared materials are highly selective and reusable catalysts.

## 1. Introduction

In the last years, mesoporous silica attracted the attention of the research and industry communities. The incorporation of mesopores into macroporous architectures provides materials where their large surface area is combined with high mass transfer [1]. Part of the attraction of these materials is mainly due to the variety of applications that they offer such as catalysis [2,3], chromatography [4], biomedicine [5–7] and environmental [8].

The sol-gel chemistry enables us to obtain nanostructured materials through a soft synthesis route. The combination of self-assembly (using macromolecular building blocks) and sol-gel processes is nowadays one of the simplest methods to develop complex but well-defined nanostructured materials with innovative properties [9]. Within this environment the formation and self-assembly of micelles occur as well as the chemical reactions of hydrolysis and condensation of the inorganic precursor that will form the oxide. Finally, the template is removed by calcination or extraction. It is possible to obtain different mesostructures with tunable properties by varying the synthesis conditions

and the nature of the template [10].

Among the most known and studied mesoporous siliceous materials are the so-called MCM-41 (Mobil Crystalline Materials No. 41) [11,12] and SBA-15 (Santa Barbara Amorphous No. 15) [13]. In some of them, the mesoporous structure is connected by the micropores on the pore walls. Different alternatives were explored to introduce an extra microporosity connecting the mesopores without changing their size and ordered structure. For example, Han et al. [14] reported the synthesis of a different mesoporous silica using TEOS as a precursor and P123 and agar as pore formers. The resulting materials showed a high BET surface area and an increase in the micropore area.

On the other hand, the heteropolyacids (HPAs) with Keggin structure are protonic acids that have complex anions called heteropolyanions. These compounds have a strong Bronsted acidity, which is an attractive property for application in acid catalysis. A low specific surface area ( $\sim 5 \text{ m}^2/\text{g}$ ) and their considerable solubility in polar solvents are the main limitations of their use. These drawbacks can be avoided if an HPA is immobilized on a suitable solid support (high specific surface area and adequate pore size), where the Keggin

\* Corresponding author.

E-mail address: [lrpizzio@quimica.unlp.edu.ar](mailto:lrpizzio@quimica.unlp.edu.ar) (L.R. Pizzio).

<https://doi.org/10.1016/j.mcat.2018.10.005>

Received 15 May 2018; Received in revised form 4 October 2018; Accepted 10 October 2018

2468-8231/ © 2018 Elsevier B.V. All rights reserved.

structure does not decompose. In addition, the resulting catalyst can easily be recovered from the reaction medium allowing it to be reused, as proposed by one of the principles of green chemistry [15].

There are different reports where HPA has been supported on zeolites, alumina, zirconia, titania and carbon [16,17]. Depending on the synthesis method, the HPAs interacting with the surface of the support can be partially decomposed, resulting in relatively low acidic materials [18,19]. Furthermore, it was reported that HPAs are more stable when they are supported on silica [20,21]. The acid features of the HPA-support materials prepared by impregnation techniques depend on the nature and stability of the species during the impregnation, drying and calcination steps [16]. We are currently exploring the use of different novel mesoporous siliceous materials, for example, core-shell polystyrene-silica and hollow silica microspheres, as HPA support for the preparation of acid catalysts [22]. To the best of our knowledge, there is only one report in which the mesoporous silica materials, synthesized according to the procedure described by Han et al., are used in an adsorption reaction [23].

In addition, benzodiazepines and their derivatives are a family of heterocyclic nitrogenous compounds of great relevance for the pharmaceutical industry [24–26] (used as anticonvulsants, anxiolytics, analgesics, anti-inflammatories, sedatives, antidepressants) and agrochemicals for the control of pests [27,28]. Generally, 3H-1,5-benzodiazepines are synthesized by the condensation reaction of *o*-phenylenediamine with ketones,  $\beta$ -haloketones and  $\alpha,\beta$ -unsaturated carbonyl compounds, using an acid catalyst. Numerous works have described their synthesis in the presence of a catalyst such as  $\text{NaBH}_4$  [29],  $\text{BF}_3\text{-OEt}_2$  [30],  $\text{Yb}(\text{OTf})_3$  [31], ionic liquid [32],  $\text{AgNO}_3$  [33],  $\text{MgO-POCl}_3$  [34],  $\text{Al}_2\text{O}_3\text{-P}_2\text{O}_5$  [35], sulfated zirconia [36], among others. In our research group, we have employed a Preyssler catalyst (bulk  $\text{H}_{14}[\text{NaP}_5\text{W}_{30}\text{O}_{110}]$ ) to obtain 3H-1,5-benzodiazepines under solvent-free conditions in order to develop a greener synthesis procedure [37].

In this work we present the synthesis of mesoporous silica materials using different agar/TEOS ratios, with the purpose of achieving a material with appropriate textural properties to be used as 12-phosphotungstic acid ( $\text{H}_3\text{PW}_{12}\text{O}_{40}$ ) support, which is claimed to be the HPA with the highest acid strength [16]. The catalytic performance of the obtained catalyst in the one-pot synthesis of 3H-1,5-benzodiazepines under solvent-free conditions is also reported.

## 2. Experimental

### 2.1. Synthesis of the support

The mesoporous silica (MESSI) samples were prepared by sol-gel chemistry using tetraethyl orthosilicate (TEOS, Sigma-Aldrich) as precursor alkoxide, the triblock copolymer P123 ( $\text{PEO}_{20}\text{PPO}_{70}\text{PEO}_{20}$ , Sigma-Aldrich) as the mesoporous template and agar (Britania) as micropore former, according to the method reported by Han et al. [14]. A series of MESSI-X samples (MESSI-0, MESSI-1, MESSI-2 and MESSI-3) was synthesized using different agar/TEOS ratio (0, 0.014, 0.028, and 0.042, respectively) with the aim of studying the effect of this variable on the textural properties of the obtained materials. For a typical synthesis of MESSI-X, 4 g of P123 was dissolved in 103 ml of 2 N aqueous HCl solution and 30 g of distilled water and stirred at 60 °C in a conical flask. When the solution became homogeneous, different amounts of agar in aqueous solution at 60 °C were added to the reaction mixture and vigorously stirred for 1 h at 60 °C. Then, 19.8 ml of TEOS was incorporated, and the solution was stirred at 700 rpm for 20 h at 90 °C. After that, the stirring was stopped and the suspension was aged for 24 h at 90 °C. The solid was isolated by filtration and washed with distilled water. Finally, the templates were removed by thermal treatment at 600 °C for 2 h.

### 2.2. Impregnation with PTA

The MESSI-2 materials were used as PTA support. The impregnation was performed by contacting, at room temperature, 0.8 g of the support with 0.2 g of 12-phosphotungstic acid ( $\text{H}_3\text{PW}_{12}\text{O}_{40}$ ) dissolved in 3 ml of water-ethanol 50% (v/v) solution in order to obtain a PTA concentration of 20% by weight in the final material (named MESSI-2PTA20). The same procedure was used to obtain samples with 30% and 40% (w/w) of PTA (MESSI-2PTA30 and MESSI-2PTA40 respectively). Finally, the solids were calcined at 200 °C for 2 h under air atmosphere. The procedure used to determine the PTA content in the calcined materials is described in the supplementary material [38].

### 2.3. Sample characterization

#### 2.3.1. Textural properties

The nitrogen adsorption/desorption measurements were carried out at liquid nitrogen temperature (77 K) using Micromeritics ASAP 2020 equipment. From the obtained data, the specific surface area ( $S_{\text{BET}}$ ) was determined using the Brunauer–Emmett–Teller model, the micropore area ( $S_{\text{MIC}}$ ) by the t-plot method and the mean pore diameter ( $D_p$ ) by the BJH method.

#### 2.3.2. Scanning electron microscopy (SEM) and transmission electron microscopy (TEM)

The morphology of the MESSI-X and MESSI-2PTA samples was characterized by SEM with Philips 505 equipment, and TEM was performed on JEOL 100 CX II equipment.

#### 2.3.3. Fourier transform infrared spectroscopy analysis (FT-IR)

The species present in the supports and catalysts were evaluated by FT-IR, using Bruker IFS 66 equipment with pellets of the sample in KBr, in the 400–4000  $\text{cm}^{-1}$  range at room temperature.

#### 2.3.4. $^{31}\text{P}$ nuclear magnetic resonance (P-NMR)

The  $^{31}\text{P}$  magic angle spinning-nuclear magnetic resonance spectra of the MESSI-2PTA20, MESSI-2PTA30 and MESSI-2PTA40 samples were collected with Bruker MSL-300 equipment (see supplementary information).

#### 2.3.5. X-ray diffraction analysis (XRD)

The structural characteristics were determined by XRD and small angle X-ray scattering (SAXS) analysis. XRD patterns were obtained employing Philips PW-1732 equipment, using  $\text{Cu K}\alpha$  radiation, Ni filter, 20 mA and 40 kV in the high voltage source, and a scanning rate of 2°/min. The SAXS measurements were performed using a laboratory SAXS setup (XEUSS 1.0, XENOCs, Grenoble) at 21 °C in the transmission configuration with variable sample-detector distance (in order to cover the angular range required for analysis).

#### 2.3.6. Acidity measurements

The acid strength and the number of acid sites were estimated from the *n*-butylamine potentiometric titration results (for more details about the technique see supplementary information).

### 2.4. Catalytic test

#### 2.4.1. Materials and methods

*o*-Phenylenediamine, sublimed (99%), 4-methyl-*o*-phenylenediamine (98%), 4-chloro-*o*-phenylenediamine (97%), 4-bromo-*o*-phenylenediamine (97%), 4-nitro-*o*-phenylenediamine 98% and 1,3-diphenyl-1,3-propanedione 98% were obtained from Sigma-Aldrich and used without further purification. The reaction was monitored by thin layer chromatography on UV-active aluminum-backed plates of silica gel (TLC Silica gel 60 F254). The  $^{13}\text{C}$ -NMR and  $^1\text{H}$ -NMR spectra were measured on a Bruker 400 MHz spectrometer in  $\text{DMSO-d}_6$ . The

chemical shift is given in ppm relative to tetramethylsilane as internal standard.

#### 2.4.2. Catalytic test for the synthesis of 3H-1,5-benzodiazepines

The catalytic tests were performed in a round bottom flask, which was equipped with a condenser and immersed in an oil bath. Then, a model experiment was carried out. To a mixture of 1,3-diphenyl-1,3-propanodione (0.25 mmol) and *o*-phenylenediamine (0.5 mmol) the solid catalyst (MESSI-2PTA30) (1% mmol of PTA relative to 1,3-diphenyl-1,3-propanodione) (total mass of catalyst = 50 mg) was added. The reaction mixture was then heated to 90 °C with stirring for 1 h. After completion (TLC control), the mixture was extracted with hot toluene (3 x 2 ml), treated with anhydrous sodium sulfate, and then the solvent was removed in vacuum at 20 °C. The solid residue was purified by silica gel column chromatography using mixtures of hexane-ethyl acetate of crescent polarity as eluent to obtain the 3H-benzodiazepine **3**. The pure benzodiazepine **3** was characterized by comparison of physical constant (retention time in TLC and melting point) using a standard sample prepared by conventional methods. In addition, the <sup>1</sup>H-NMR and <sup>13</sup>C-NMR were determined. A large-scale experiment was performed using 5 mmol of 1,3-diphenyl-1,3-propanodione, and the results were similar to those obtained on a reduced scale.

#### 2.4.3. Catalyst stability and reuse test

For catalyst recycling studies, the used solid catalyst was washed with 4 ml of toluene, after its filtration from the reaction media, and dried in vacuum at 90 °C up to constant weight. More than 95% of the catalyst mass was recovered after each reuse.

#### 2.4.4. <sup>1</sup>H NMR and <sup>13</sup>C NMR spectra of selected synthesized compounds

**Compound 3a:** <sup>1</sup>H NMR (400 MHz, DMSO-d<sub>6</sub>): δ 3.72 (br s, 2H); 7.38 (dd, 2H, J = 3 Hz, 6 Hz); 7.40–7.47 (6H, m); 7.62 (dd, 2H, J = 3 Hz, 6 Hz); 7.99–8.01 (4H, m). <sup>13</sup>C NMR (100 MHz, DMSO-d<sub>6</sub>): δ 35.3, 125.6, 128.4, 128.6, 128.7, 130.9, 137.6, 140.7, 154.2.

**Compound 3b:** <sup>1</sup>H RMN (400 MHz, DMSO-d<sub>6</sub>): δ 2.60 (s, 3H); 3.72 (br s, 2H); 7.24–7.30 (m, 2H); 7.41–7.51 (m, 7H); 7.96–8.05 (m, 4H). <sup>13</sup>C NMR (100 MHz, DMSO-d<sub>6</sub>): δ 18.7, 35.0, 125.9, 126.5, 128.1, 128.2, 128.8, 128.7, 129.3, 130.4, 130.8, 136.3, 137.4, 137.5, 139.1, 140.8, 151.8, 153.9.

**Compound 3c:** <sup>1</sup>H NMR (400 MHz, DMSO-d<sub>6</sub>): δ 3.70 (br s, 2H); 7.33 (dd, 1H, J = 2.3 Hz, 8.4 Hz); 7.42–7.47 (m, 6H); 7.56 (dd, 1H, J = 0.45 Hz, 8.4 Hz); 7.63 (dd, 1H, J = 0.45 Hz, J = 2.3 Hz); 7.97–8.00 (m, 4H). <sup>13</sup>C NMR (100 MHz, DMSO-d<sub>6</sub>): δ 35.5, 125.8, 128.1, 128.2, 128.2, 128.6, 130.1, 130.4, 129.5, 130.9, 131.3, 136.9, 137.1, 139.3, 141.6, 154.4, 154.9.

**Compound 3d:** <sup>1</sup>H NMR (400 MHz, DMSO-d<sub>6</sub>): δ 3.80 (br s, 2H); 6.87–6.92 (m, 1H); 7.02 (dd, 1H, J = 8.0 Hz, J = 1.14 Hz), 7.35–7.45 (m, 3H); 7.47–7.52 (m, 3H); 7.58 (dd, 1H, J = 7.2 Hz, J = 2.0 Hz); 7.68 (dd, 1H, J = 7.2 Hz, J = 2.0 Hz); 7.85 (dd, 1H, J = 8.0 Hz, J = 2.0 Hz); 8.04–8.07 (m, 2H); 14.52 (s, 1H). <sup>13</sup>C NMR (100 MHz, DMSO-d<sub>6</sub>): δ 33.4, 118.0, 118.6, 118.6, 125.9, 126.7, 128.0, 128.4, 128.5, 128.8, 129.3, 131.0, 133.6, 136.8, 137.5, 141.7, 155.5, 158.5, 162.6.

### 3. Results and discussion

#### 3.1. Catalyst characterization

The N<sub>2</sub> adsorption–desorption isotherms of MESSI-X are shown in Fig. 1, and the most important textural data are listed in Table 1. MESSI-X isotherms that can be classified as type IV (with H<sub>2</sub> hysteresis loops). The main features of the isotherms remain unchanged no matter the agar/TEOS ratio employed during the synthesis.

The specific surface area (S<sub>BET</sub>) values are higher than 600 m<sup>2</sup>/g and increase with the increment of the agar/TEOS ratio used in the synthesis (Table 1). The S<sub>BET</sub> value of MESSI-1 is 11% higher than that of

MESSI-0 (agar/TEOS ratio increases from 0 to 0.014). This increment is mainly due to the increase in the mesopore area (S<sub>MIC</sub> remains practically constant). On the other hand, only a slight increment of S<sub>BET</sub> (3%) takes place when the agar/TEOS ratio increases from 0.0014 to 0.028. However, the micropore area increases by ~25%. The use of a higher ratio (0.042) during the synthesis produces a material with practically the same specific surface area and a lower S<sub>MIC</sub> value (712 and 142 m<sup>2</sup>/g respectively). Taking into account that the micropores present in this kind of material facilitate the mass transfer among the mesopores, we selected the MESSI-2 material as support for the immobilization of PTA.

The S<sub>BET</sub> values of MESSI-2PTA20, MESSI-2PTA30, and MESSI-2PTA40 (Table 1) significantly decrease due to the heteropolyacid addition. It could be mainly due to the mesopores blocking of MESSI-2 by the incorporated PTA anion (which has a diameter of 1.2 nm). Additionally, the slow decrease in parallel with the increment of PTA can be explained considering that the specific surface area of bulk PTA is very low (7 m<sup>2</sup>/g), and that MESSI-2PTA materials are composed of 20%, 30%, and 40% of PTA respectively. On the other hand, S<sub>MIC</sub> remains practically unchanged and D<sub>p</sub> slightly increases.

The SEM micrographs of MESSI-2 sample (Fig. 2a) show that the material is formed by agglomerates of particles of spherical shape, whose diameter varies from 1.2 to 5 μm. Furthermore, this morphology does not change after the addition of PTA to the support (Fig. 2b). EDX mapping images of Si (line K) and W (line L) elements (Fig. 2c and d respectively) show that they are approximately homogeneously distributed in the MESSI-2PTA30 sample. Similar features are displayed by the MESSI-2PTA20 and MESSI-2PTA40 samples. So the synthesized samples present an adequate dispersion of heteropolyacid throughout the material.

The spherical particles seem to be formed by aggregation of small nanoparticles that, according to the TEM micrographs (Fig. 3), present a worm-like structure. This type of image corresponds to a short-range arrangement as is reported in [39,40].

The MESSI-X samples present typical XRD patterns corresponding to silica materials with amorphous structure, with two wide bands centered at around 2θ = 12 and 22°. The MESSI-X samples were subjected to SAXS analysis. In all cases the SAXS patterns show an intense peak corresponding to the (100) plane diffraction (corresponding to an interplanar spacing of 10.5 nm) and two less intense peaks assigned to (110) and (200) planes. The positions of these peaks are characteristic of a 2D hexagonal pore array (P6mm symmetry). However, the not well resolved peaks assigned to (110) and (200) planes can be due to a short extension 2D hexagonal pore array (Fig. 4).

Furthermore, SAXS patterns and TEM images of MESSI-2PTA samples reveal that the mesoporous structure remains unchanged after the impregnation with PTA and subsequent calcination.

The XRD patterns of MESSI-2PTA are shown in Fig. 5. MESSI-2PTA20 and MESSI-2PTA30 patterns present the same features as the MESSI-2 support. When 40% of PTA was incorporated into the support, very low intensity peaks assignable to H<sub>3</sub>PW<sub>12</sub>O<sub>40</sub>·6H<sub>2</sub>O are observed at around 2θ = 8°, 19°, and 27°. These results suggest that PTA is well dispersed on the support as a noncrystalline phase or present as crystals with a size not detectable by this technique.

The FT-IR spectra of the MESSI-2, PTA and mesoporous silica supported PTA samples are shown in Fig. 6.

The FT-IR spectra of MESSI-2 sample exhibit the main characteristic bands of silica (Table 2, entry 1–6) and do not show any of those belonging to the organic compounds used as pore-forming agent (agar and P123).

MESSI-2PTA samples exhibit the listed bands of PTA (Table 2, entry 7–11) overlapping those of the support [41]. Furthermore, with the increase of PTA loading in the samples, the intensity of the bands assigned to the heteropolyacid clearly increases. On the other hand, neither the characteristic bands of the lacunary anion [PW<sub>11</sub>O<sub>39</sub>]<sup>7-</sup> nor those of the dimeric anion [P<sub>2</sub>W<sub>21</sub>O<sub>71</sub>]<sup>6-</sup> are observed [42]. These results confirm that the [PW<sub>12</sub>O<sub>40</sub>]<sup>3-</sup> anion is the main species in the

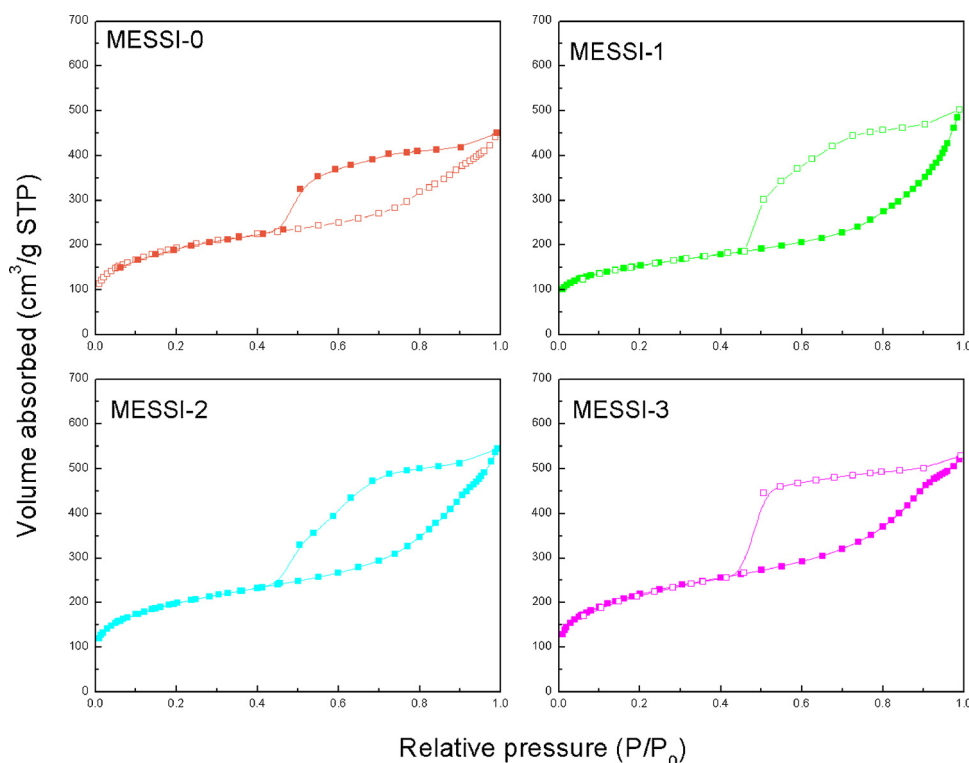


Fig. 1. N<sub>2</sub> adsorption–desorption isotherms of MESSI-X.

**Table 1**  
Textural properties and size of MESSI-X and MESSI-2PTAY.

Sample	Agar/TEOS ratio	S <sub>BET</sub> (m <sup>2</sup> /g)	S <sub>MIC</sub> (m <sup>2</sup> /g)	D <sub>p</sub> (nm)
MESSI-0	0	622	126	4.6
MESSI-1	0.014	691	129	4.6
MESSI-2	0.028	710	161	4.9
MESSI-3	0.042	712	142	4.4
PTA	–	7	–	1.2
MESSI-2PTA20	0.028	335	88	5.0
MESSI-2PTA30	0.028	269	86	4.8
MESSI-2PTA40	0.028	180	72	5.7

MESSI-2PTA samples, so we can suggest that the Keggin structure of PTA is not lost during the impregnation and calcination processes.

The <sup>31</sup>P magic angle spinning-nuclear magnetic resonance spectra of MESSI-2PTA20, MESSI-2PTA30, and MESSI-2PTA40 samples (Fig. 7a–c, respectively) display a line at -14.8 ppm, which was attributed to [H<sub>x</sub>PW<sub>12</sub>O<sub>40</sub>]<sup>(3-x)-</sup> species [43,44]. Moreover, the <sup>31</sup>P NMR spectrum of MESSI-2PTA40 sample shows a second and less intense line at -15.1 ppm ascribed to the [PW<sub>12</sub>O<sub>40</sub>]<sup>3-</sup> Keggin anion [45] interacting with H<sup>+</sup>(H<sub>2</sub>O)<sub>2</sub> species [46,47]. In the case of hydrated PTA (H<sub>3</sub>PW<sub>12</sub>O<sub>40</sub>·6H<sub>2</sub>O) this line appears at -15.3 ppm. The downfield shift observed, compared to that of the PTA, was due to the electrostatic interaction among the anions and the ≡Si–OH<sub>2</sub><sup>+</sup> groups present in MESSI-2PTA samples. A similar behavior was suggested for the interaction of PTA with zirconia and titania [44].

The potentiometric titration with n-butylamine let us estimate the number of acid sites and the acid strength of the solids. According to the titration curves (Fig. 8) MESSI-2, MESSI-2PTA20, MESSI-2PTA30, MESSI-2PTA40 and PTA exhibit E<sub>i</sub> values higher than 100 mV (144, 570, 530, 730 and 764 mV respectively) assigned to the presence of very strong acid sites (see supplementary material). Besides, the area under the curve increases significantly as a result of PTA incorporation to the support, following the order: MESSI-2 < < MESSI-2PTA20 < MESSI-2PTA30 < MESSI-2PTA40 (71, 101, 148, 184 meg n-

butylamine/g, respectively). The acid strength and the number of sites increase with the increment of the PTA amount in the samples.

### 3.2. Catalytic tests

Initially, the optimum reaction conditions were checked employing 1,3-diphenyl-1,3-propanedione and 1,2-phenylenediamine as test reaction substrates under solvent-free conditions (Scheme 1). Various reaction conditions were studied: temperature, reaction time, amount of catalyst, and molar ratio of substrates (Table 4).

The blank experiment, without the presence of catalyst, gives only traces (< 5%) of benzodiazepine **3a** (Table 3, entry 1). Similarly, the support MESSI-2 gives a poor yield of 28% of the product (Table 3, entry 2). The reaction conditions were temperature, 90 °C, and reaction time, 1 h. We evaluated the catalytic performance of bulk PTA in the reaction between o-phenylenediamine and 1,3-diphenyl-1,3-propanedione. A low reaction yield was obtained (18%) due to the low specific surface area of bulk PTA (7 m<sup>2</sup>/g), despite its high acid strength.

Then, we tested the MESSI-2PTA20, MESSI-2PTA30, and MESSI-2PTA40 materials as catalysts, and it can be seen that the yields increase with the increase of the PTA content (MESSI-2PTA20 < MESSI-2PTA30 < MESSI-2PTA40) (Table 3, entries 3, 4 and 5). However, no relevant yield differences are obtained between catalyst MESSI-2PTA30 and MESSI-2PTA40 (70% and 72% respectively). For this reason, MESSI-2PTA30 was chosen to be used in the following experiments because a lower amount of PTA is required for its synthesis.

It is well known that the reaction is reversible, so in the following experiments we explored the molar relationship between the reactants (Table 3). Although the yields are good when the reactants react in an equimolar ratio (63%, Table 3, entry 6), they rise to 70% when using a 2:1 excess ratio of the diamine substrate (Table 3, entry 4). No relevant changes were obtained when the diamine was used in an excess ratio of 3:1 (Table 3, entry 7). The 2:1 diamine/dione ratio was used in the next experiment.

Then, we explored the effect of the reaction temperature. Four additional experiments were performed at 110, 90, 50 and 25 °C using

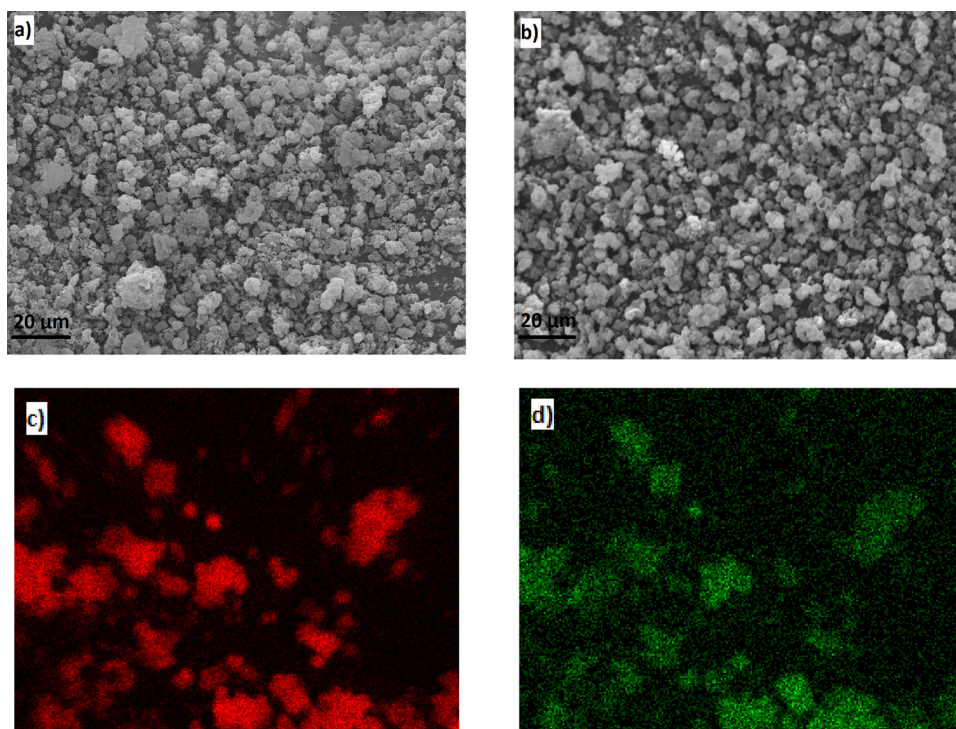


Fig. 2. a) SEM image (Magnification 500x) of MESSI-2, b) SEM image (Magnification 500x) of MESSI-2PTA30, Elemental mapping images of the MESSI-2PTA30 sample c) Si mapping, d) W mapping.

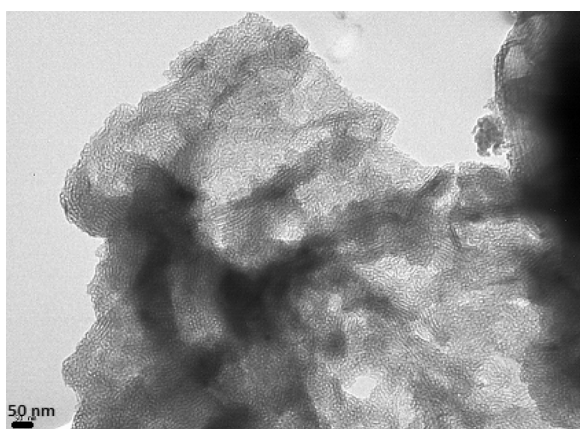


Fig. 3. TEM images of MESSI-2PTA30.

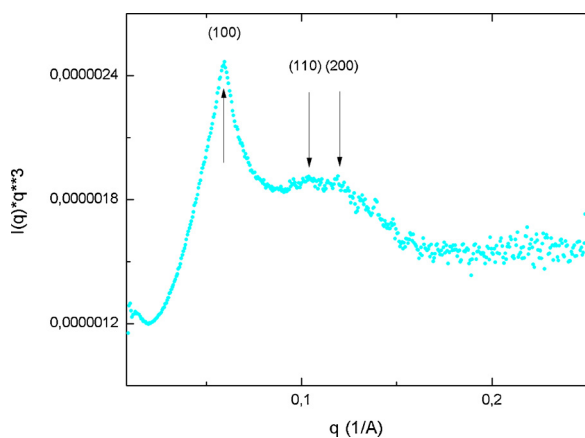


Fig. 4. SAXS of MESSI-2.

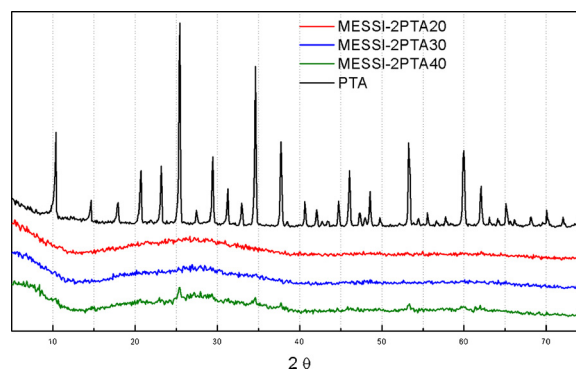


Fig. 5. DRX patterns of MESSI-2, MESSI-2PTAY and PTA.

MESSI-2PTA30 (1 mmol % of active phase) (Table 3). No reaction was detected when the reaction temperature was 25 °C (Table 3, entry 10). The experiment lasted 3 h. The results show that the best yield was obtained at 90 °C (72%, Table 3, entry 4) and similar yields were obtained at 110 °C (74%, Table 3, entry 8). However, one secondary product (not identified) was detected by TLC. A temperature of 90 °C was used in the next experiments.

Another relevant factor in these catalytic tests is the amount of MESSI-2PTA30. Table 3 shows the results when different amounts of MESSI-2PTA30 were added to the reaction mixture at the previously defined optimal conditions. It can be seen that 1 mmol % (15 mg of active phase) of MESSI-2PTA30 gives good yields (70%, Table 3, entry 4) and no changes were obtained when the increase in the catalyst amount was 2 mmol % (70%, Table 3, entry 12).

Finally, we investigated the reaction time, at the selected optimal temperature of 90 °C, using four different times of 0.5, 1 and 2 h (Table 3). A yield of 58% was obtained at 0.5 h (Table 3, entry 13) reaching the optimal yields at 1 h (72%, Table 3, entry 4), without any variation at longer reaction times (2 h, 71%, Table 3, entry 14).

Table 4 shows the results from the study on the reusability of the

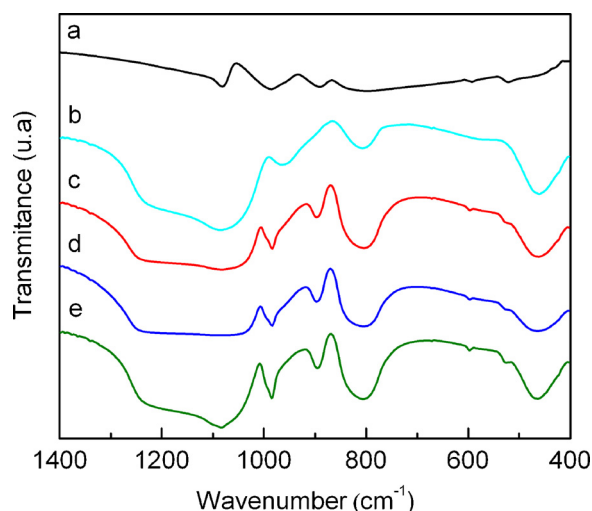


Fig. 6. FT-IR spectra of a) PTA, b) MESSI-2, c) MESSI-2PTA20, d) MESSI-2PTA30, e) MESSI-2PTA40.

Table 2

FT-IR characteristic bands of MESSI-2 and PTA.

Entry	Vibration modes	Band ( $\text{cm}^{-1}$ )
1	Stretching OH group	3700–3200
2	Angular vibration $\text{H}_2\text{O}$	1650
3	Asymmetric stretching siloxane group	1220–1076
4	Stretching Si–OH group	965
5	Stretching Si–O–Si group	800
6	Bending O–Si–O group	470
7	Stretching vibrations P–Oa	1081
8	Stretching vibrations W=Od	982
9	Stretching vibrations W–Ob–W	888
10	Stretching vibrations W–Oc–W	793
11	Bending vibration Oa–P–Oa	524

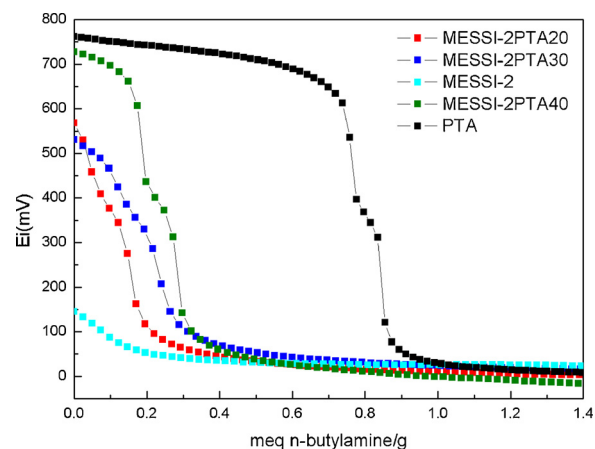


Fig. 8. Potentiometric titration curves.

catalyst MESSI-2PTA30. The recovered catalyst was reused under similar reaction conditions and reactant content (90 °C, under solvent-free conditions, with 15 mg of PTA (active phase) and a 1:2 dione/diamine ratio), over four consecutive tests. No appreciable variation of the reaction yields was detected. More than 90% of the catalyst mass was recovered after each test.

To explore the scope and generality of benzodiazepine synthesis, a variety of *o*-phenylenediamines containing substituents in aromatic ring such as -H, 3- $\text{CH}_3$ , 4-Cl, 4-Br and 4- $\text{NO}_2$  were reacted with 1,3-diphenyl-1,3-propanodione. The reaction yields for each benzodiazepine 3a-3e are listed in Table 3. In general, in most of the studied cases, the reaction proceeded smoothly to give good to excellent yields of the desired 1,5 benzodiazepines (Table 5). However, strongly electron-withdrawing groups such as - $\text{NO}_2$  electron-deficient aromatic rings dramatically decrease the nucleophilicity of amines, and the reaction does not take place.

#### 4. Conclusions

Summarizing, mesoporous silica (MESSI) materials were prepared

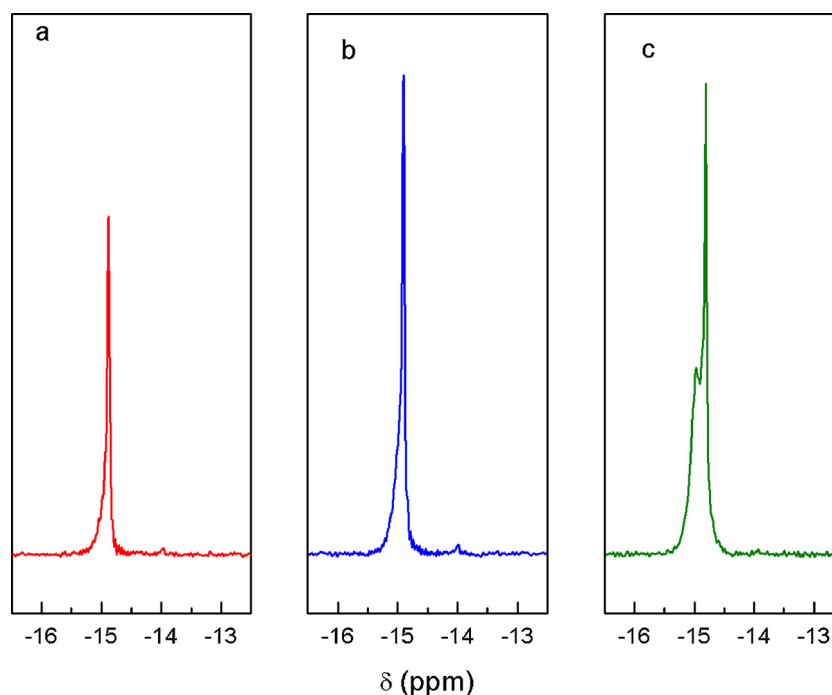
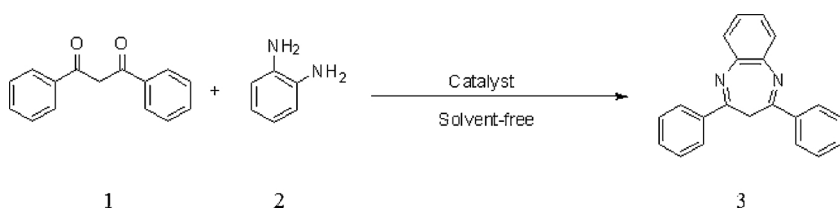


Fig. 7.  $^{31}\text{P}$  MAS NMR spectra of a) MESSI-2PTA20, b) MESSI-2PTA30, c) MESSI-2PTA40.



**Scheme 1.** Condensation reaction between 1,3-diphenyl-1,3-propanedione and 1,2-phenylenediamine.

**Table 3**

Catalytic test to the reaction between *o*-phenylenediamine and 1,3-diphenyl-1,3-propanedione.

Entry	CAT	% CAT	Temp (°C)	Time (h)	Rel A/D <sup>a</sup>	Y (%) <sup>b</sup>
1	–	1	90	1	2/1	5
2	MESSI-2	1	90	1	2/1	28
3	MESSI-2PTA20	1	90	1	2/1	58
4	MESSI-2PTA30	1	90	1	2/1	70
5	MESSI-2PTA40	1	90	1	2/1	72
6	MESSI-2PTA30	1	90	1	1/1	63
7	MESSI-2PTA30	1	90	1	3/1	71
8	MESSI-2PTA30	1	110	1	2/1	74
9	MESSI-2PTA30	1	50	3	2/1	30
10	MESSI-2PTA30	1	25	3	2/1	–
11	MESSI-2PTA30	0.5	90	1	2/1	60
12	MESSI-2PTA30	2	90	1	2/1	70
13	MESSI-2PTA30	1	90	0.5	2/1	58
14	MESSI-2PTA30	1	90	2	2/1	71

Reaction condition: 1,3-diphenyl-1,3-propanodione (0.25 mmol); *o*-phenylenediamine (0.5 mmol); catalyst; solvent-free; stirring.

a A/D: ratio between diamine and dione compound.

bPure product.

**Table 4**

Catalyst reuse.

Entry	Cicle	Yields (%)
1	Use	70
2	1st Reuse	68
3	2sc	68
4	3th	67

Reaction condition: 1,3-diphenyl-1,3-propanodione (0.25 mmol); *o*-phenylenediamine (0.5 mmol); catalyst (1 mmol %); solvent-free; temperature, 90 °C; time, 1 h; stirring.

using agar and P123 as pore-forming agents. The agar/TEOS ratio influences the specific surface area ( $S_{\text{BET}}$ ) and the micropore area ( $S_{\text{MIC}}$ ). SAXS patterns and TEM images of MESSI samples reveal the presence of a 2D hexagonal mesopore array. The mesoporous structure remains unchanged after the impregnation with PTA and the thermal treatment.

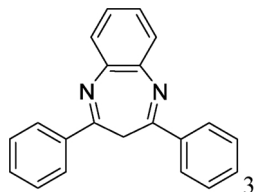
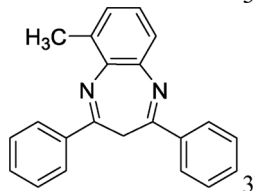
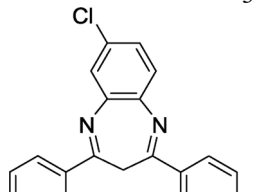
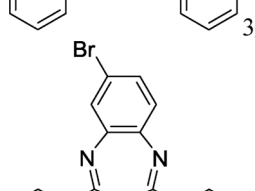
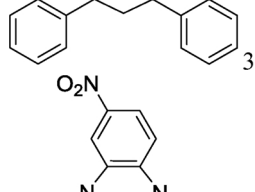
In the MESSI-2PTA materials, the FT-IR and  $^{31}\text{P}$  MAS NMR characterizations show the presence of the undegraded  $[\text{PW}_{12}\text{O}_{40}]^{3-}$  and  $[\text{H}_x\text{PW}_{12}\text{O}_{40}]^{(3-x)-}$  species interacting electrostatically with the  $\equiv\text{Si}-\text{OH}_2^+$  groups present in the MESSI-2 support. Furthermore, potentiometric titration showed the presence of very strong acid sites in all the synthesized solids.

A series of substituted 3*H*-1,5-benzodiazepines were synthesized from 1,3-propanediones and 1,2-phenylenediamine using MESSI-2PTA materials under solvent-free reaction conditions.

This methodology requires a short reaction time of 60 min, and a temperature of 90 °C, to obtain very good yields of derivatives. Taking into account the results shown in this work, the mesoporous silica materials impregnated with PTA present suitable physicochemical properties to be used as catalysts in the synthesis of 1,5-benzodiazepine derivatives from a multicomponent condensation reaction, under solvent-free conditions.

**Table 5**

3*H*-Benzodiazepines synthesis using MESSI-2PTA30 as catalyst.

Entry	Product	Yield (%)
1		70
2		75
3		68
4		67
5		–

Reaction condition: 1,3-diphenyl-1,3-propanodione (0.25 mmol); substituted *o*-phenylenediamine (0.5 mmol); catalyst (1 mmol %); solvent-free; temperature, 90 °C; time, 1 h; stirring.

## Acknowledgements

We thank Universidad Nacional de La Plata, CONICET and ANPCyT for financial support and L. Osiglio, M. Theiller and J. Tara for their collaboration in the experimental measurements.

## Appendix A. Supplementary data

Supplementary material related to this article can be found, in the online version, at doi:<https://doi.org/10.1016/j.mcat.2018.10.005>.

## References

- [1] X.Y. Zhang, D.X. Liu, D.D. Xu, S. Asahina, K.A. Cychosz, K.V. Agrawal, Y.A. Wahedi, A. Bhan, S.A. Hashimi, O. Terasaki, M. Thommes, M. Tsapatsis, Synthesis of self-pillared zeolite nanosheets by repetitive branching, *Science* 336 (2012) 1684–1687.
- [2] P. Hu, W.Z. Lang, X. Yan, X.F. Chen, Y.J. Guo, Vanadium-doped porous silica materials with high catalytic activity and stability for propane dehydrogenation reaction, *Appl. Catal. A Gen.* 553 (2018) 65–73.
- [3] M. Eslami, M.G. Dekamin, L. Motlagh, A. Maleki, MCM-41 mesoporous silica: a highly efficient and recoverable catalyst for rapid synthesis of  $\alpha$ -aminonitriles and imines, *Green Chem. Lett. Rev.* 11 (2018) 36–46.
- [4] L.F. Giraldo, B.L. Lopez, L. Perez, S. Urrego, L. Sierra, M. Mesa, Mesoporous silica applications, *Macromol. Symp.* 258 (2007) 129–141.
- [5] Y. Teng, Y. Jiang, Y. Zhang, X. Xu, K. Lin, Controlled-release drug carriers based mesoporous silica spheres with hierarchical hollow/nano structure, *J. Porous Mater.* 24 (2017) 241–248.
- [6] X. Yang, D. He, X. He, K. Wang, J. Tang, Z. Zou, X. He, J. Xiong, L. Li, J. Shangguan, Synthesis of hollow mesoporous silica nanorods with controllable aspect ratios for intracellular triggered drug release in Cancer cells, *ACS Appl. Mater. Interfaces* 8 (2016) 20558–20569.
- [7] J.G. Croissant, Y. Fatieiev, N.M. Khashab, Degradability and clearance of silicon, Organosilica, Silsesquioxane, silica mixed oxide, and mesoporous silica nanoparticles, *Adv. Mater.* 29 (2017) 1–51.
- [8] D. Lei, Q. Zheng, Y. Wang, H. Wang, Preparation and evaluation of aminopropyl-functionalized manganese-loaded SBA-15 for copper removal from aqueous solution, *J. Environ. Sci.* 28 (2015) 118–127.
- [9] G.J.A.A. Soler-Illia, O. Azzaroni, Multifunctional hybrids by combining ordered mesoporous materials and macromolecular building blocks, *Chem. Soc. Rev.* 40 (2011) 1107–1150.
- [10] R. Deshmukh, M. Niederberger, Nonhydrolytic Sol–Gel methods, in: D. Levy, M. Zayat (Eds.), *The Sol-Gel Handbook*, E-publishing Inc., New York, 2015, pp. 29–69.
- [11] C.T. Kresge, M.E. Leonowicz, W.J. Roth, J.C. Vartuli, J.S. Beck, Ordered mesoporous molecular sieves synthesized by a liquid-crystal template mechanism, *Nature* 359 (1992) 710–712.
- [12] J.S. Beck, J.C. Vartuli, W.J. Roth, M.E. Leonowicz, C.T. Kresge, K.D. Schmitt, C.T.W. Chu, D.H. Olson, E.W. Sheppard, A new family of mesoporous molecular sieves prepared with liquid crystal templates, *J. Am. Chem. Soc.* 114 (1992) 10834–10843.
- [13] D. Zhao, J. Feng, Q. Huo, N. Melosh, G.H. Fredrickson, B.F. Chmelka, G.D. Stucky, Triblock copolymer syntheses of Mesoporous Silica with periodic 50 to 300 angstrom pores, *Science* 279 (1998) 548–552.
- [14] Y. Han, J. Choi, M. Tong, H. Kim, Synthesis and characterization of high-surface-area millimeter-sized silica beads with hierarchical multi-modal pore structure by the addition of agar, *Mater. Charact.* 90 (2014) 31–39.
- [15] P.T. Anastas, J.C. Warner, Principles of green chemistry, in: P.T. Anastas (Ed.), *Green Chemistry: Theory and Practice*, E-publishing Inc., New York, 1998, pp. 1–132.
- [16] L.R. Pizzio, C.V. Cáceres, M.N. Blanco, Acid catalysts prepared by impregnation of tungstophosphoric acid solutions on different supports, *Appl. Catal. A Gen.* 167 (1998) 283–294.
- [17] Y.P. Wijaya, H.P. Winoto, Y.K. Park, D.J. Suh, H. Lee, J.M. Ha, J. Jae, Heteropolyacid catalysts for Diels-Alder cycloaddition of 2,5-dimethylfuran and ethylene to renewable p-xylene, *Catal. Today* 293 (2017) 167–175.
- [18] K.M. Rao, R. Gobetto, A. Iannibello, A. Zecchina, Solid state NMR and IR studies of phosphomolybdenum and phosphotungsten heteropoly acids supported on  $\text{SiO}_2$ ,  $\gamma\text{-Al}_2\text{O}_3$ , and  $\text{SiO}_2\text{-Al}_2\text{O}_3$ , *J. Catal.* 119 (1989) 512–516.
- [19] G.I. Kapustin, T.R. Brueva, A.L. Klyachko, M.N. Timofeeva, S.M. Kulikov, I.V. Kozhevnikov, A study of the acidity of heteropoly acids, *Kinet. Katal.* 3 (1990) 1017–1020.
- [20] J.B. Moffat, S. Kasztelan, The Oxidation of methane on heteropolyoxometalates, Nature and stability of the supported species, *J. Catal.* 109 (1988) 206–211.
- [21] S. Kasztelan, E. Payen, J.B. Moffat, The formation of molybdosilicic acid on Mo/ $\text{SiO}_2$  catalysts and its relevance to methane oxidation, *J. Catal.* 112 (1988) 320–324.
- [22] M.N. Gorsd, M.N. Blanco, L.R. Pizzio, Polystyrene/silica microspheres with core/shell structure as support of tungstophosphoric acid, *Mater. Chem. Phys.* 171 (2016) 281–289.
- [23] Y. Han, G. Hwang, H. Kim, B.Z. Haznedaroglu, B. Lee, Amine-impregnated millimeter-sized spherical silica foams with hierarchical mesoporous–macroporous structure for  $\text{CO}_2$  capture, *Chem. Eng. J.* 259 (2015) 653–662.
- [24] Y. Xie, W.V. Lane, R.H. Loring, Nereistoxin: a naturally occurring toxin with redox effects on neuronal nicotinic acetylcholine receptors in chick retina, *J. Pharmacol. Exp. Ther.* 264 (1993) 689–694.
- [25] A. Kato, M. Ichimaru, Y. Hashimoto, H. Mitsudera, Guinesine-A, -B and -C: new sulfur containing insecticidal alkaloids from *Cassipourea guianensis*, *Tetrahedron Lett.* 30 (1989) 3671–3674.
- [26] I. Dell, C.R.A. Godfrey, D.J. Wadsworth, D.R. Baker, J.G. Fenyes, Synthesis and chemistry of agrochemicals, in: J.J. Steffens (Ed.), *ACS Symposium Series*, 1992, p. 384 Washington DC.
- [27] H. Yanagawa, T. Kato, Y. Kitahara, Asparagusic acid-S-oxides new plant growth regulators in etiolated young asparagus shoots, *Tetrahedron Lett.* 13 (1973) 1073–1075.
- [28] W.D. Celmer, F.W. Tanner, M. Harfenist, T.M. Lees, I.A. Solomons, Characterization of the antibiotic thiolutin and its relationship with aureothricin, *J. Am. Chem. Soc.* 74 (1952) 6304–6305.
- [29] H.R. Morales, A. Bulbarel, R. Contreras, New synthesis of dihydro- and tetrahydro-1,5-benzodiazepines by reductive condensation of o-phenylenediamine and ketones in the presence of sodium borohydride, *Heterocycles* 24 (1986) 135–139.
- [30] J.A.L. Herbert, H. Sushitzky, Syntheses of heterocyclic compounds. Part XXIX. Substituted 2,3-dihydro-1H-1,5-benzodiazepines, *J. Chem. Soc. Perkin Trans. I* 1 (1974) 2657–2661.
- [31] M. Curini, F. Epifano, M.C. Marcotullio, O. Rosati, Ytterbium triflate promoted synthesis of 1,5-benzodiazepine derivatives, *Tetrahedron Lett.* 42 (2001) 3193–3195.
- [32] D.V. Jarikote, S.A. Siddiqui, R. Rajagopal, T. Daniel, R.J. Lahoti, K.V. Srinivasan, Room temperature ionic liquid promoted synthesis of 1,5-benzodiazepine derivatives under ambient conditions, *Tetrahedron Lett.* 44 (2003) 1835–1838.
- [33] R. Kumar, P. Chaudhary, S. Nimesh, A.K. Verma, R. Chandra, An efficient synthesis of 1,5-benzodiazepine derivatives catalyzed by silver nitrate, *Green Chem.* 8 (2006) 519–521.
- [34] M.S. Balakrishna, B. Kaboudin, A simple and new method for the synthesis of 1,5-benzodiazepine derivatives on a solid surface, *Tetrahedron Lett.* 42 (2001) 1127–1129.
- [35] B. Kaboudin, K. Navaee, Alumina/phosphorus pentoxide (APP) as an efficient reagent for the synthesis of 1,5-benzodiazepines under microwave irradiation, *Heterocycles* 55 (2001) 1443–1446.
- [36] B.M. Reddy, P.M. Sreekanth, An efficient synthesis of 1,5-benzodiazepine derivatives catalyzed by a solid superacid sulfated zirconia, *Tetrahedron Lett.* 44 (2003) 4447–4449.
- [37] G.A. Pasquale, D.M. Ruiz, J.L. Jios, J.C. Autino, G.P. Romanelli, Preyssler catalyst-promoted rapid, clean, and efficient condensation reactions for 3H-1,5-benzodiazepine synthesis in solvent-free conditions, *Tetrahedron Lett.* 54 (2013) 6574–6579.
- [38] A.A. Sosa, M.N. Gorsd, M.N. Blanco, L.R. Pizzio, Synthesis and characterization of tungstophosphoric acid-modified mesoporous silica nanoparticles with tuneable diameter and pore size distribution, *J. Sol-Gel Sci. Technol.* 83 (2017) 355–364.
- [39] O. Adetola, I. Little, R. Mohseni, D. Molodyi, S. Bohvan, L. Golovko, A. Vasiliev, Synthesis of mesoporous silica gels with embedded heteropolyacids, *J. Sol-Gel Sci. Technol.* 81 (2017) 205–213.
- [40] H. Iván Meléndez-Ortiz, B. Puente-Urbina, G. Castruita-deLeon, J.M. Mata-Padilla, L. García-Uriostegui, Synthesis of spherical SBA-15 mesoporous silica. Influence of reaction conditions on the structural order and stability, *Ceram. Int.* 42 (2016) 7564–7570.
- [41] L.R. Pizzio, P.G. Vázquez, C.V. Cáceres, M.N. Blanco, Supported Keggin type heteropolycompounds for ecofriendly reactions, *Appl. Catal. A Gen.* 256 (2003) 125–139.
- [42] L.R. Pizzio, M.N. Blanco, A contribution to the physicochemical characterization of nonstoichiometric salts of tungstosilicic acid, *Mater. Lett.* 61 (2007) 719–724.
- [43] R. Massart, R. Contant, J. Fruchart, J. Ciabrini, M. Fournier, Phosphorus-31 NMR studies on molybdic and tungstic heteropolyanions, Correlation between structure and chemical shift, *Inorg. Chem.* 16 (1977) 2916–2921.
- [44] J.A. Rengifo-Herrera, M.N. Blanco, J. Wist, P. Florian, L.R. Pizzio,  $\text{TiO}_2$  modified with polyoxotungstates should induce visible-light absorption and high photocatalytic activity through the formation of surface complexes, *Appl. Catal. A Gen. B: Environ.* 189 (2016) 99–109.
- [45] F. Lefebvre,  $^{31}\text{P}$  MAS NMR study of  $\text{H}_3\text{PW}_{12}\text{O}_{40}$  supported on silica: Formation of  $(=\text{SiOH}_2^+)(\text{H}_2\text{PW}_{12}\text{O}_{40}^-)$ , *J. Chem. Soc. Chem. Commun.* 10 (1992) 756–757.
- [46] N. Essayem, Y.Y. Tong, H. Jobic, J.C. Vedrine, Characterization of protonic sites in  $\text{H}_3\text{PW}_{12}\text{O}_{40}$  and  $\text{Cs}_{1.9}\text{H}_{1.1}\text{PW}_{12}\text{O}_{40}$ : a solid-state  $^1\text{H}$ ,  $^2\text{H}$ ,  $^{31}\text{P}$  MAS-NMR and inelastic neutron scattering study on samples prepared under standard reaction conditions, *Appl. Catal. A-Gen.* 194 (2000) 109–122.
- [47] T. Okuhara, T. Nishimura, H. Watanabe, K. Na, M. Misono, Novel catalysis of cesium salt of heteropoly acid and its characterization by solid-state NMR, *Stud. Surf. Sci. Catal.* 90 (1994) 419–428.